RSC Advances

PAPER

View Article Online
View Journal | View Issue

Cite this: *RSC Adv.*, 2017, **7**, 51374

Rieche formylation of carbon nanotubes – one-step and versatile functionalization route†

Anna Kolanowska,[a] Anna Kuziel,[a] Yuliu Li,[a] Sebastian Jurczyk[b] and Sławomir Boncel *[a]

Received 22nd September 2017
Accepted 24th October 2017

DOI: 10.1039/c7ra10525h

rsc.li/rsc-advances

We present the direct and one-step Rieche formylation of carbon nanotubes (CNTs) as the most effective (4.00 mmol g^{-1}) functionalization route *via* formylation. Indeed, classical methods, *i.e.* three-step protocols based on CNT oxidation–reduction–partial oxidation (COOH ≫ CH_2OH ≫ CHO), were revealed as less effective and more troublesome. All CNT-CHO products were comprehensively analysed by cross-verified potentiometric titration, scanning electron microscopy (SEM), thermogravimetry (TGA), Fourier transform infrared spectroscopy (FT-IR) and Raman spectroscopy.

Introduction

Exohedral functionalization of carbon nanotubes (CNTs)—inspired by organic chemistry—has opened up numerous toolboxes toward CNT applications in various fields, from electronics to materials engineering to medicine.[1] Typically, the CNT-anchored functional groups or nanoparticles provide better dispersibility in solvents and enhanced compatibility with polymer (or metal or ceramic) matrices. Consequently, this approach makes CNTs processable and conducive to a 'properties-by-design' approach.[2] Those physicochemical CNT outer-shell modifications include several methods—leading to nanotube disentanglement and individualization—based on the formation of non-covalent and covalent bonds.[3] Among the latter, *i.e.* the ones most influencing the electronic and morphological skeleton of CNTs, several different methods have been reported, and they are predominantly based on oxidation using HNO_3,[4] nitrating mixtures,[5] $KMnO_4$,[6] H_2O_2 [7] or O_3.[8] Furthermore, a number of other CNT reactions with radicals,[9–11] cycloadditions,[12–15] and electrophilic additions[16–18] have also been studied. Nevertheless, in total, the aforementioned oxidation has been, by now, undeniably the most frequently and widely used method to alter/tune the physicochemistry of CNTs. This fact derives from usually high functionalization degrees, as well as the convenience and versatility of the introduced carboxyl (–COOH) and hydroxyl (–OH) groups as the anchoring points, mainly for further covalent modifications.[19] This approach, however, induces defects in the nanotube walls, decreases the nanotube aspect ratio (nanotubes can be cut) and consequently aggravates the mechanical and electrical properties of CNTs; oxidized CNTs also become hydrophilic.[20] As for non-destructive treatments, Tessonnier *et al.*[21] reported the modification of CNTs with tertiary amino groups without the oxidation step. The procedure involved deprotonation–lithiation/carbometalation reaction followed by an electrophilic substitution by 2-(diethylamino)ethyl bromide. In this two-step approach, concentration of the 3°-amino functional groups was found to be 1 mmol g^{-1}; nonetheless, the method did not require harsh conditions.

In the quest for alternative routes, we have turned to a synthetic precursor of the carboxyl group, *i.e.*, the aldehyde group, which might emerge as even more powerful – indeed, the high and multi-target reactivity of aldehydes (RCHO) locates them among the most important organic compounds. Definitely, the formyl group (–CHO) appears as a powerful surface modifier, as it constitutes a convenient starting point for the synthesis of alcohols,[22,23] amines,[24,25] acids,[26] oximes,[27,28] alkenes,[29,30] alkynes,[31] epoxides,[32,33] *etc.* Therefore, formylation of CNTs is a natural synthetic route to practically countless post-modifications of formylated CNTs that are susceptible to many readily available nucleophiles. However, to our extreme surprise, literally just one synthetic strategy of CNT formylation has been applied to date,[34,35] *i.e.*, the pre-formation of lithiated CNTs (CNT anion = 'carbon nanotubide') and their subsequent reaction with *N*-formylpiperidine (which is, formally, transfer of the formyl group).

In order to explore new areas of CNT chemistry—against the background of organic chemistry methods that have been reserved mainly for aromatic low-molecular-weight molecules—we report on studies of CNT formylation. Herein, so as to perform direct (one-step) formylation of CNTs, we have elaborated a protocol based on Rieche formylation, *i.e.* employing dichloromethyl methyl ether (Cl_2CHOCH_3) as a formylating agent in the presence of $TiCl_4$ as Lewis acid. The intermediate product in this reaction is an unstable α-alkoxybenzyl chloride which further

[a]*Silesian University of Technology, Department of Organic Chemistry, Bioorganic Chemistry and Biotechnology, Krzywoustego 4, 44-100 Gliwice, Poland. E-mail: slawomir.boncel@polsl.pl; Fax: +48 32 237 20 94; Tel: +48 32 237 12 72*

[b]*Institute for Engineering of Polymer Materials and Dyes, Skłodowskiej-Curie 55, 87-100 Toruń, Poland*

† Electronic supplementary information (ESI) available. See DOI: 10.1039/c7ra10525h

decomposes to yield exclusively the appropriate aldehyde. Nevertheless, application of the Rieche reaction could be a challenge, as it was initially reserved for activated aromatic compounds bearing electron-donating groups. Hence, it could provide higher functionalization levels, but only for suitably pre-activated CNTs. On the other hand, one might expect that MWCNTs, as metallic tubes, could be more susceptible to the attack of reactive electrophiles.[36,37] In order to place the above hypothesis in the appropriate context, for comparative purposes, as the commonly applied alternative approach, CNTs were initially oxidized (the first general step) to CNT-COOH, which was further reduced with lithium aluminium hydride (LAH) to hydroxymethyl-CNTs (CNT-CH_2OH). The resulting hydroxymethyl groups were oxidized to the formyl ones using CrO_3, $K_2Cr_2O_7$ or HBr.

Experimental

Materials

MWCNTs (9.6 nm diameter, 1.5 μm length, 90% purity) were purchased from Nanocyl, Belgium. Longer and thicker in-house MWCNTs were synthesized by catalytic chemical vapour deposition (c-CVD) (a detailed procedure is presented in ESI†). SEM images of in-house MWCNTs (see further) showed that most of them had a diameter ranging between 60–70 nm and length up to 200 μm. Single-walled CNTs (SWCNTs) were purchased from TUBALL™ (Luxembourg) and were used additionally as the important model nanotubes. General characteristics of all CNTs used in the work are presented in Table 1. $LiAlH_4$ (95%), $HBr_{(aq)}$ (48%, ACS reagent), DMSO (>99%), $TiCl_4$ (>99%), dichloromethyl methyl ether (98%), CaH_2 (pure p.a.), ferrocene ($FeCp_2$) (98%), and NH_2OH HCl (99%) from Sigma-Aldrich, Poland; H_2SO_4 (95%, pure p.a.), HNO_3 (65%, pure p.a.), HCl (35–38%, pure p.a.), NaOH (pure p.a.), anhydrous $MgSO_4$ (pure p.a.), $NaHCO_3$ (pure p.a.), Na_2CO_3 (pure p.a.), and toluene (pure p.a.) from Chempur, Poland; and CrO_3 (pure), $K_2Cr_2O_7$ (pure), and KBr (pure) from Avantor Performance Materials, Poland, were used as received. Prior to use, methylene chloride and toluene were extracted with conc. H_2SO_4, saturated $NaHCO_{3(aq)}$ solution and water, dried with anhydrous $MgSO_4$, and then distilled from CaH_2. Filtrations were performed using PTFE filters (Merck Milipore pore size 0.2 μm).

Synthesis of carboxy-MWCNTs (MWCNT-COOH)

MWCNTs (5.00 g) were treated with a mixture of HNO_3 : H_2SO_4 (1 : 3; v/v) (128 mL). The reaction mixture was refluxed for 10 min, with the vigorous evolution of NO_2. Next, after cooling down to room temperature (2 h), the oxidized nanotubes were filtered off. Subsequently, MWCNT-COOH was rinsed thoroughly with water until pH = 7. MWCNT-COOH was dried at 85 °C for 12 h. The reaction scheme is presented in Fig. 1.

Table 1 Characterization of CNTs

Properties	Nanocyl NC7000™	In-house MWCNTs	TUBALL™ SWCNTs
Average diameter, nm	9.5	60–70	1.6
Average length, μm	1.5	200	>5
Aspect ratio	150	3000	3000
Carbon purity, wt%	90	98	85
Fe-based catalyst residue, wt%	<1	5.4	<15

Reduction of MWCNT-COOH to hydroxymethyl-MWCNTs (MWCNT-CH_2OH) [modified procedure from ref. 38]

To a magnetically stirred, 250 mL three-necked, round-bottomed flask containing MWCNT-COOH (1.00 g) and $LiAlH_4$ (0.50 g), and equipped with: (1) a drying pipe (cont. $CaCl_2$), (2) a dropping funnel, and (3) an Ar balloon, anhydrous toluene (150 mL) was added over 30 min. The reaction mixture was stirred for 24 h. Then, the reaction mixture was quenched, and MWCNT-CH_2OH was filtered off and rinsed with 2 M HCl_{aq} (50 mL). MWCNT-CH_2OH was washed thoroughly with water until neutral pH of the filtrate. The resulting material was dried at 85 °C overnight. The reaction scheme is presented in Fig. 2.

Partial oxidation of MWCNT-CH_2OH to formyl-MWCNTs (MWCNT-CHO)

Method 1 [modified procedure from ref. 39 for aromatic compounds]. To a magnetically stirred dispersion of MWCNT-CH_2OH (0.20 g) in DMSO (25 mL) in a round-bottomed flask equipped with a reflux condenser, a solution of CrO_3 (0.50 g) in DMSO (5 mL) was added dropwise over 5 min. After stirring for 4 h at room temperature, cold distilled water (100 mL) was added to the reaction mixture, and the product was filtered off. MWCNT-CHO was washed with water (100 mL) and acetone (50 mL) until a colourless filtrate was observed. The resulting material was dried at 85 °C overnight. The reaction scheme is presented in Fig. 3.

Method 2 [modified procedure from ref. 40 for aromatic compounds]. MWCNT-CH_2OH (0.20 g), $K_2Cr_2O_7$ (1.00 g) and DMSO (25 mL) were placed in a round-bottomed flask equipped with a reflux condenser. The mixture was heated at 100 °C for 4 h. After cooling down to room temperature, the product was filtered off. MWCNT-CHO was washed with water (100 mL) and acetone (50 mL) until a colourless filtrate was observed. The resulting material was dried at 85 °C overnight. The reaction scheme is presented in Fig. 4.

Method 3 [modified procedure from ref. 41 for aromatic compounds]. A mixture of MWCNT-CH_2OH (0.20 g), 48% HBr_{aq} (0.5 mL) and DMSO (20 mL) was magnetically stirred in an oil bath at 100 °C for 4 h. After cooling down to room temperature,

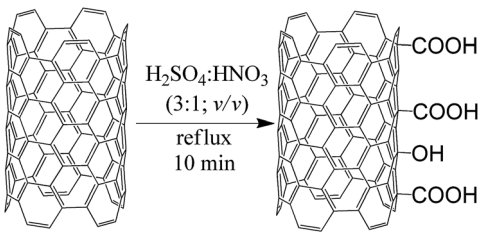

Fig. 1 Procedure for synthesis of MWCNT-COOH.

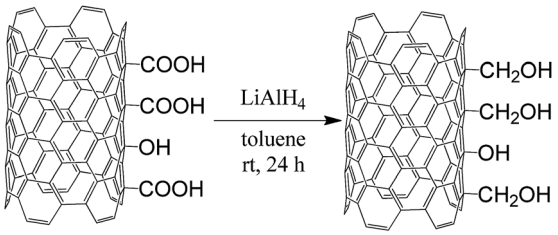

Fig. 2 Procedure for reduction of MWCNT-COOH to hydroxymethyl-MWCNTs (MWCNT-CH_2OH).

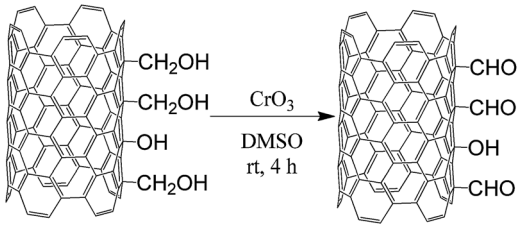

Fig. 3 Procedure for partial oxidation of MWCNT-CH_2OH to formyl-MWCNTs (MWCNT-CHO) using chromium trioxide (CrO_3) in DMSO.

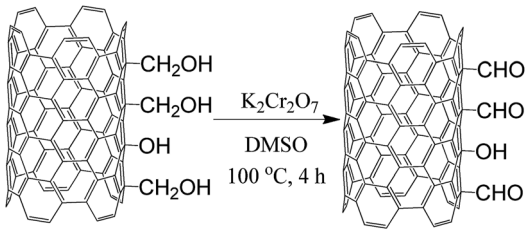

Fig. 4 Procedure for partial oxidation of MWCNT-CH_2OH to formyl-MWCNTs (MWCNT-CHO) with potassium dichromate ($K_2Cr_2O_7$) in DMSO.

the product was filtered off. MWCNT-CHO was washed with water (100 mL) and acetone (50 mL) until a colourless filtrate was observed. The resulting material was dried at 85 °C overnight. The reaction scheme is presented in Fig. 5.

Rieche formylation of MWCNTs

To a round-bottomed flask cooled to 0 °C containing MWCNTs (1.00 g) and dichloromethyl methyl ether (1.5 mL) in anhydrous CH_2Cl_2 (50 mL), $TiCl_4$ (1 mL) was added dropwise under N_2, and the mixture, under the above conditions, was magnetically stirred for 1 h.[42] The stirring was continued at room temperature for 20 h. The product was filtered off. MWCNT-CHO precursor was washed with water (100 mL) and acetone (50 mL) until a colourless filtrate was observed. The resulting material was dried at 85 °C overnight. The reaction scheme is presented in Fig. 6.

Characterization

Scanning electron microscopy (SEM), titration, thermogravimetry (TGA), Fourier transform infrared (FTIR) spectroscopy and

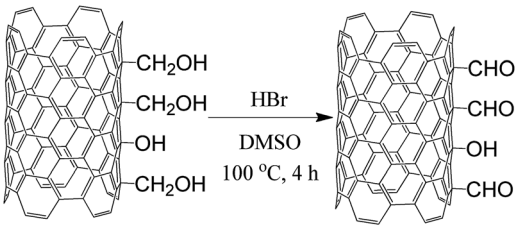

Fig. 5 Procedure for oxidation of MWCNT-CH_2OH to formyl-MWCNTs (MWCNT-CHO) with hydrobromic acid (HBr_{aq}) in DMSO.

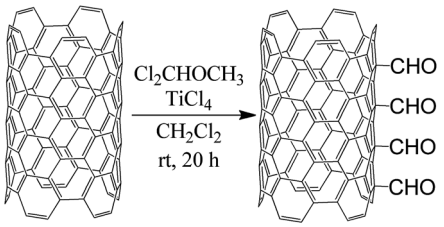

Fig. 6 Rieche formylation of CNTs.

Raman spectroscopy were used to characterize the changes in morphology and surface physicochemistry of functionalized CNTs. SEM images were taken on Hitachi TM3000. Samples were analyzed at 5 kV with a working distance of 4.5 mm. TGA curves were recorded under nitrogen using a TGA/DSC1 Mettler-Toledo at a heating rate of 10 °C min^{-1}. FTIR spectra were acquired using a Specord M80 (KBr pellet – 0.5 mg CNTs/1 g KBr, 500–4000 cm^{-1} range). Raman spectra were obtained using a InVia Renishaw at 633 nm (He/Ne laser).

The content of CNT surface oxygen groups was determined by Boehm titration,[43] and the procedure was as follows: functionalized MWCNTs (60 mg) were dispersed for 48 h under continuous stirring in the specified aqueous reaction base solutions: (1) freshly prepared 0.01 M NaOH, 60 mL; (2) 0.01 M Na_2CO_3, 30 mL; (3) 0.01 M $NaHCO_3$, 60 mL. The mixture was filtered, then 10 mL (or 5 mL in the case of Na_2CO_3) of the filtrates was titrated with 0.01 M HCl_{aq} (20 mL). The pH of the final solutions was measured using a pH meter (EcoTestr 2). Each titration was performed in triplicate. As blank samples, 10 mL of each reaction base (5 mL in the case of Na_2CO_3) was used. For quantification of surface formyl groups in CNT-CHO, reaction of the aldehyde groups with hydroxylamine was used (Fig. 7): a given MWCNT sample (20 mg) and hydroxylamine hydrochloride (35 mg) solution in water (50 mL) were ultrasonicated for 5 min. Then, the analyzed mixture was heated to 60 °C and kept at this temperature for 20 min. The evolved HCl was titrated with 0.01 M $NaOH_{aq}$. Each titration was performed in triplicate. A schematic of the titration setup is presented in Fig. 8.

Results and discussion

Morphology of CNT-CHO *versus* unmodified CNTs

The morphology of CNTs and their functionalized counterparts was analyzed by SEM; Fig. 9 shows SEM micrographs for pristine

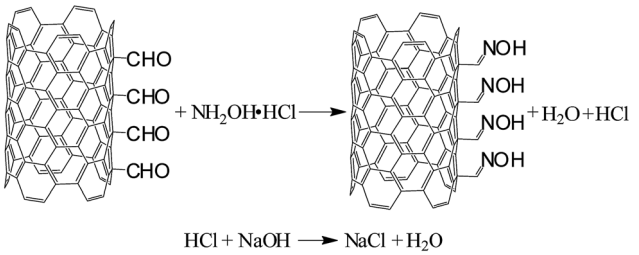

Fig. 7 Reactions during quantification of the formyl groups in CNT-CHO determined by potentiometric titration—formation of CNT-oximes with a simultaneous release of hydrogen chloride.

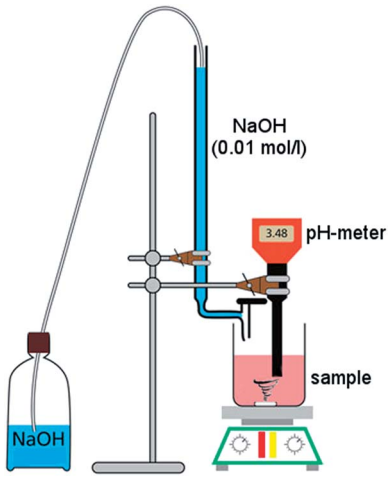

Fig. 8 Setup of the titration experiment.

Nanocyl™, in-house and TUBALL™ Fig. 9(a, b, c) and formylated CNTs. Nanocyl MWCNTs were found as highly twisted and entangled nanoparticles forming nearly spherical (cauliflower-like) agglomerates. In contrast, in-house MWCNTs (of the highest diameter) and TUBALL™ SWCNTs, due to the similar and high aspect ratio (3000) among the studied CNTs, were visible as mostly vertically aligned tubes forming separate icelands ('carpets') and sets of fibrils, respectively. Further, Fig. 9(d–g) show formylated Nanocyl™, Fig. 9(h–k) formylated in-house MWCNTs and Fig. 9(l) formylated TUBALL™. As can be seen, none of the treatments have led to alteration of the nanotube morphology, leaving the nanotube intact on the microscale. Critically, in light of the results on effective functionalization presented later—as well as from the further application point of view—CNTs after Rieche formylation procedure also remained unchanged (long and straight tubes are present) and also, due to a straightforward one-step protocol, practical lack of impurities could be observed. This comparison has important consequences for three-step formylation procedures, which potentially generate more extensive additional contamination.

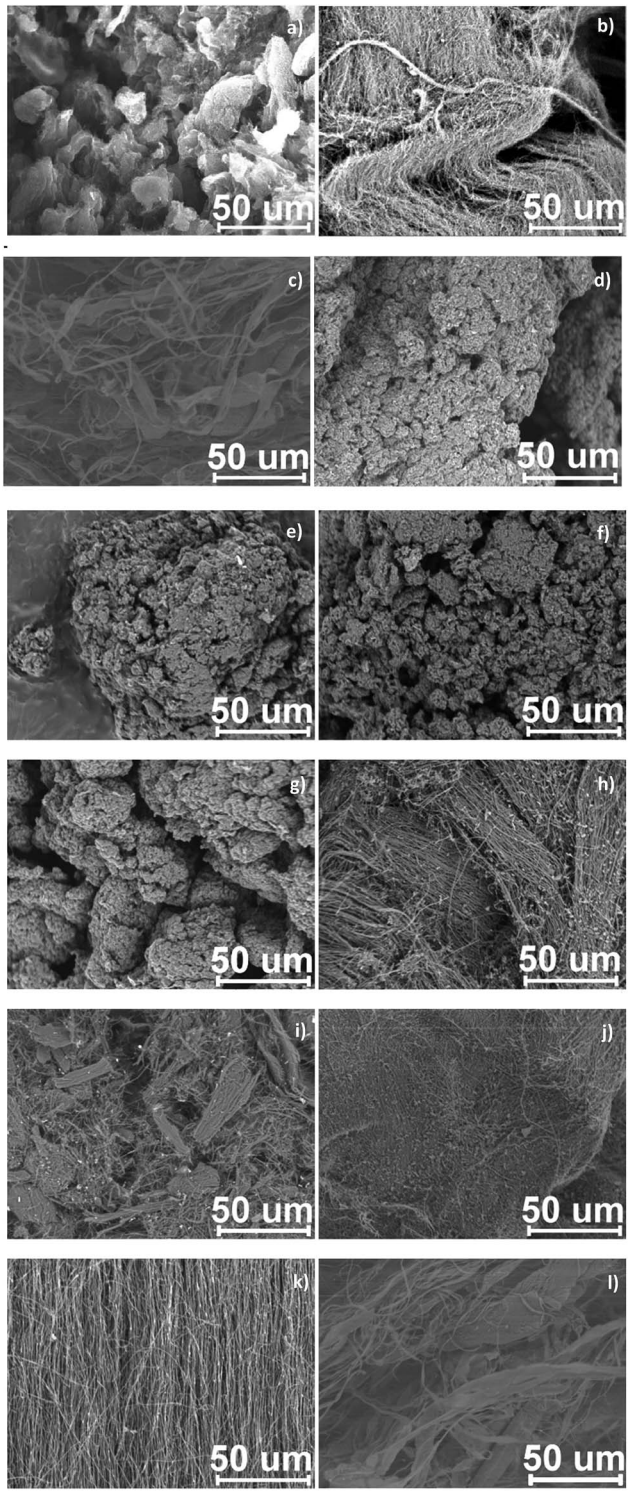

Fig. 9 SEM images of CNTs: (a) Nanocyl™ MWCNTs, (b) in-house MWCNTs, (c) TUBALL™ SWCNTs, (d) f-Nanocyl™ by CrO_3/DMSO, (e) f-Nanocyl™ by $K_2Cr_2O_7$/DMSO, (f) f-Nanocyl™ by HBr/DMSO, (g) f-Nanocyl™ by Cl_2CHOCH_3, $TiCl_4$, (h) f-in-house by CrO_3/DMSO, (i) f-in-house by $K_2Cr_2O_7$/DMSO, (j) f-in-house by HBr/DMSO, (k) f-in-house by Cl_2CHOCH_3, $TiCl_4$, (l) f-TUBALL™ by Cl_2CHOCH_3, $TiCl_4$.

FTIR spectroscopy

Fig. 10 shows the FTIR spectra of SWCNTs before (black line) and after (red line) Rieche formylation. For pristine SWCNTs, the bands at 3450 (ν_{O-H}) and 1262 cm^{-1} (ν_{C-O}) could be attributed to the presence of surface hydroxyl groups, which are believed to result from ambient atmospheric moisture bound to

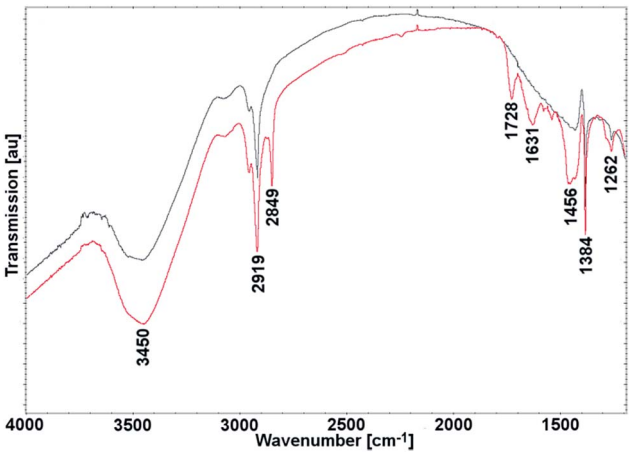

Fig. 10 FTIR spectra of SWCNTs, (black) before and (red) after direct formylation.

the outermost SWCNT shells.[44] Nota bene, the presence of surface hydroxyl groups activates the graphene wall to the electrophilic attack.

For the formylated SWCNTs, two new bands appeared at 1728 and 2849 cm^{-1}. The emergence of an absorption peak at 1728 cm^{-1} in the FTIR spectrum of functionalized SWCNTs is a clear indication of carbonyl (C=O) groups. The peak can be assigned to the C=O stretching vibration ($\nu_{C=O}$). Importantly, a peak at 2849 cm^{-1} corresponds to asymmetrical stretching vibrations of O=C–H bonds in aldehydes (ν_{C-H}). Bands at around 3000, 1631, 1456, and 1384 cm^{-1} are connected with the aromatic structure of CNTs. Weak signals at *ca.* 3000 cm^{-1} correspond to stretching vibrations of C_{Ar}–H (ν_{C-H}). Skeletal vibrations, involving carbon–carbon stretching within the ring, absorbed energy at 1631, 1456 and 1384 cm^{-1} ($\nu_{C=C}$). Two very weak bands between 1456 and 1384 cm^{-1} can be attributed to overtone bands.

Quantification of carboxyl groups and formyl groups in CNT-CHO *via* titration

The amount of carboxyl groups was calculated as follows:

$$n_{COOH} = \frac{C_{HCl}\left(V^0_{HCl} - V_{HCl}\right)}{m_{CNTs}}$$

where C_{HCl} – concentration of the titrant [mol L^{-1}], V^0_{HCl} – volume of the titrant in blank titration [mL], V_{HCl} – volume of the titrant [mL], m_{CNTs} – amount of CNTs used for the titration analysis [g].

The concentrations of the determined formyl groups for CNT samples after formylation are summarized in Table 2.

Degree of functionalization was calculated using the equation:

$$n_{CHO} = \frac{V_{NaOH}C_{NaOH} - V^0_{NaOH}C_{NaOH}}{m_{CNTs}\left[\frac{mmol}{g}CNTs\right]}$$

where V_{NaOH} – volume of the titrant [mL], C_{NaOH} – molar concentration of the titrant [mol L^{-1}], V^0_{NaOH} – volume of the titrant in blank titration [mL], m_{CNTs} – amount of CNTs used for the titration analysis [g].

Table 2 The carboxyl group content in MWCNT samples after –COOH to –CHO conversion as determined by titration[b]

Functionalising agent in DMSO	Functionalization degree [mmol COOH g^{-1} CNTs]			
	Nanocyl™ NC7000		In-house	
	Before[a]	After[a]	Before[a]	After[a]
$K_2Cr_2O_7$	3.0 ± 0.10	1.0 ± 0.12	1.5 ± 0.08	0.50 ± 0.02
CrO_3		1.0 ± 0.09		0.30 ± 0.01
HBr		0.5 ± 0.04		0.80 ± 0.01

[a] Before – titration for MWCNT-COOH; after – titration for MWCNT-CHO. [b] In the case of Rieche formylation, no carboxyl groups were detected.

The determined concentrations of the formyl groups in CNT samples after formylation are summarized in Table 3.

The influence of dichloromethyl methyl ether concentration on the functionalization degree was further verified by titration of the Rieche-formylated Nanocyl MWCNTs, and the results are presented in Fig. 11. It can be seen that at lower concentration of the electrophile, with its increasing concentration, degree of functionalization has also increased, with a linear dependence. But when concentration of the ether was higher than 16 mmol g^{-1} CNTs, only a slight further increase in the functionalization level could be observed, indicating saturation of the MWCNT active sites. Those reactive hot-spots could be ascribed to the graphene wall defects. This relationship proves the quantitative tunability of this type of functionalization.

Thermogravimetric analyses

In order to further confirm functionalization degrees in CNT-CHO, TG analyses were performed in argon atmosphere (Fig. 12). It can be assumed that the weight loss above 300 °C could be ascribed to the actual quantity of covalently bonded formyl groups (temperature of decarbonylation of aromatic compounds and above the range for volatilization of water and organic solvents). This characteristic was exploited in other studies.[45,46] The weight loss in the range 320–360 °C corresponds to thermal decarbonylation in the CNT-CHO, in which formyl groups were covalently attached to the CNT walls.[35] Therefore, functionalization degrees were calculated by a projection of the peak onset and offset points in derivative thermogravimetry (DTG) curves onto the corresponding TGA curves. The as-estimated functionalization degrees are presented in Table 4.

The highest functionalization degrees were observed for the CNT samples after Rieche formylation, the lowest for Nanocyl™ NC7000 after $K_2Cr_2O_7$ and in-house after HBr/DMSO. SWCNTs and shorter/thinner Nanocyl™ NC7000 were more reactive in formylation reactions than longer and thicker in-house MWCNTs. The obtained values fully correspond with the values determined by titration. Additionally, the conversion of

Table 3 The formyl group content in Rieche-formylated CNTs in comparison with alternatively synthesized CNT-CHO *via* the 'COOH ≫ CH_2OH ≫ CHO' route as determined by titration

Functionalising agent in DMSO	Functionalization degree [mmol g^{-1} CNTs]		
	Nanocyl™ NC7000	In-house	TUBALL™
$K_2Cr_2O_7$	1.90 ± 0.06	1.00 ± 0.03	—
CrO_3	1.96 ± 0.05	1.14 ± 0.03	—
HBr	2.38 ± 0.07	0.75 ± 0.02	—
Cl_2CHOCH_3, $TiCl_4$	3.68 ± 0.11	1.25 ± 0.04	4.00 ± 0.12

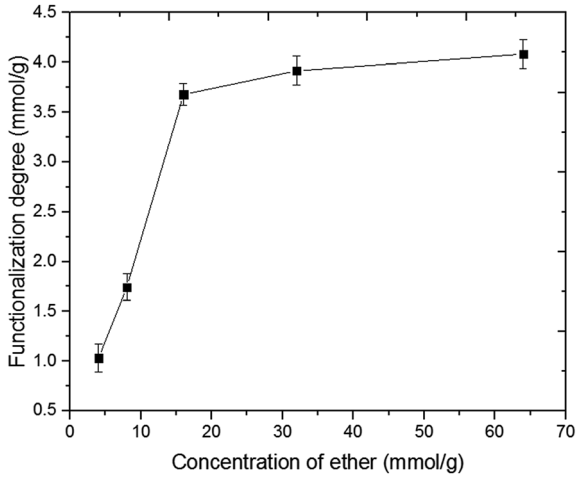

Fig. 11 Effect of the ether concentration (mmol g^{-1} MWCNTs) on the functionalization degree with formyl groups; the line serves as the eye-guide only; the titrations for each measuring point were performed in triplicate.

carboxyl to formyl groups was incomplete and ranged from 47 to 67%. In comparison, in formylation studies presented by Bayazit *et al.*,[34] *N*-formylpiperidine has been used for the transfer of formyl groups to lithiated SWCNTs. The authors have observed for SWCNT-CHO in the TG curves weight loss of 25 wt% (with 5 wt% for purified SWCNT). However, at the same time, they have claimed that each introduction of the formyl group caused a simultaneous introduction of an 'ortho-located' *n*-butyl group. Hence, the actual degree of functionalization as counted solely per formyl group was in fact lower, *i.e.* approximately 2–3 mmol g^{-1}.

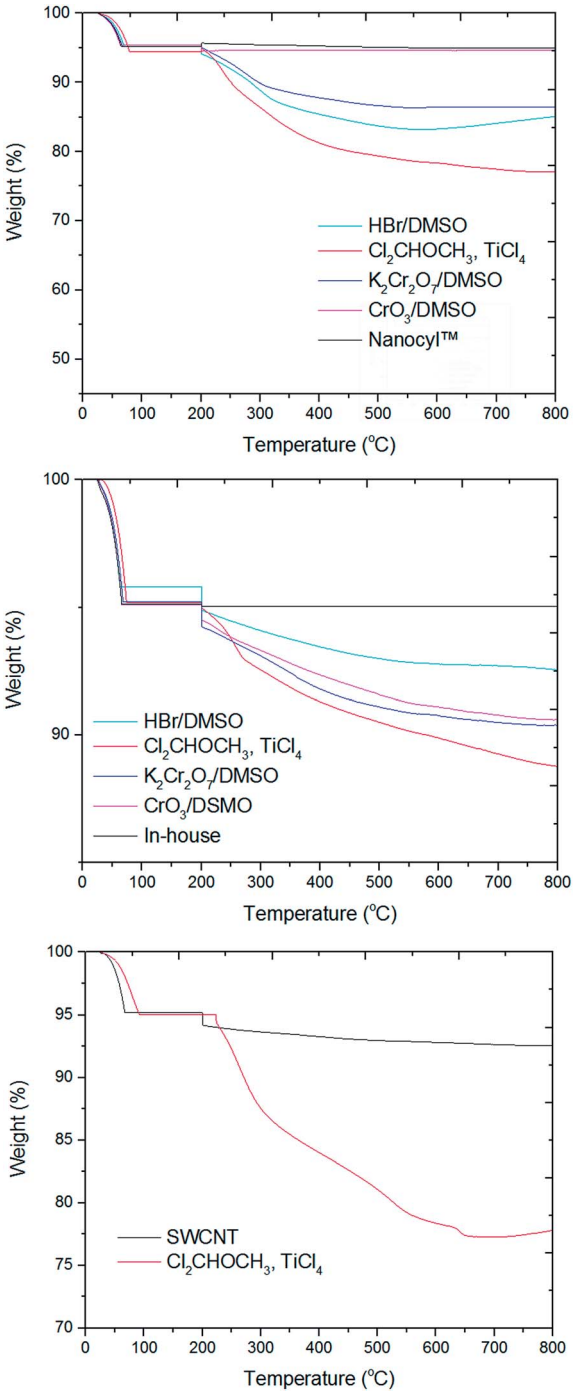

Fig. 12 Representative TGA plots for pristine (Nanocyl™ NC7000, in-house and TUBALL™) *versus* formylated CNTs using different functionalizing agents.

Raman characterization of SWCNTs *vs.* SWCNT-CHO

The Raman spectrum of SWCNTs basically contains four characteristic features. Radial breathing mode (RBM) can be generally found between 100–400 cm^{-1}.[47] The feature in the region between 1500–1600 cm^{-1} is related to tangential G-mode and is an intrinsic feature in all sp^2-carbon materials. Lineshape of the G-band differs in accordance with whether the nanotubes are semiconducting or metallic.[48] The Raman feature around 1350 cm^{-1} corresponds to disorder-induced D-mode. The D-band involves scattering from defects that break the basic symmetry of the graphene sheet, and it is observed in sp^2-carbons containing porous fraction, impurities, functionalization or other defects.[49] The Raman spectrum also contains a band at 2500–2700 cm^{-1} (G′-band), and it depends on the diameter of CNT.[50]

Here, the Raman spectrum (Fig. 13) of formylated SWCNTs (SWCNT-CHO) (B) were found as significantly different from that of pristine SWCNTs (A). With respect to the tangential

Table 4 Functionalization degrees (mmol g^{-1} CNTs) estimated from TGA for CNT-CHO

	Functionalization degree [mmol g^{-1} CNTs]		
Functionalising agent	Nanocyl™ NC7000	In-house	TUBALL™
$K_2Cr_2O_7$, DMSO	1.76	0.94	—
CrO_3, DMSO	1.81	0.94	—
HBr, DMSO	2.37	0.67	—
Cl_2CHOCH_3, $TiCl_4$	3.66	1.12	3.90

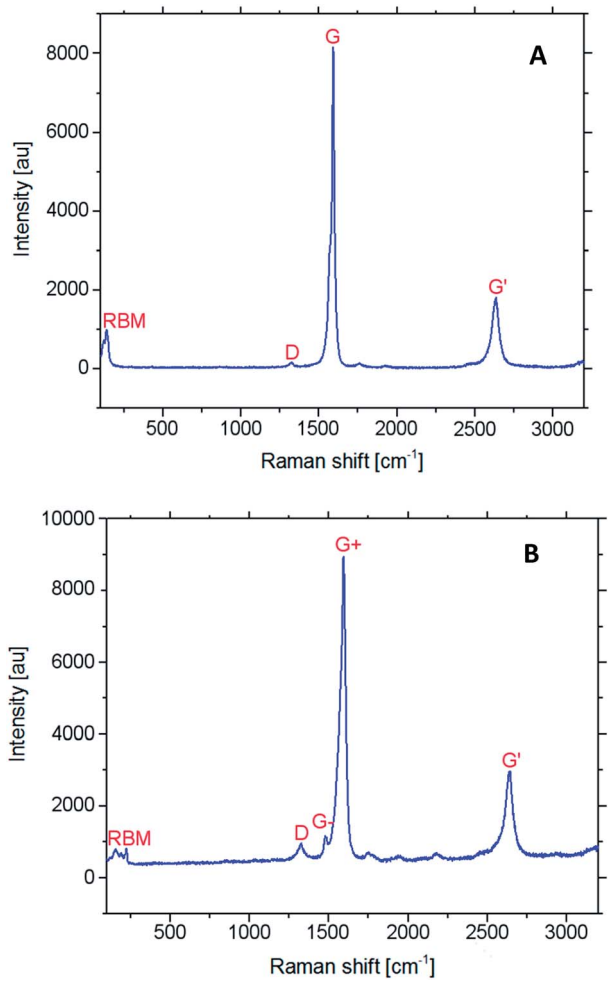

Fig. 13 Raman spectra of SWCNTs: (A) before and (B) after formylation.

mode at 1593 cm^{-1} (G-band), the intensity of the disorder peak at 1330 cm^{-1} (D-band) has changed significantly in SWCNT-CHO, and the I_D/I_G ratio increased from *ca.* 0.02 to 0.11, indicating conversion of sp^2-to sp^3-carbons in formyl-SWCNT. The disorder mode involves the resonance-enhanced scattering of an electron *via* phonon emission, which is induced by defects breaking the basic symmetry of the graphene plane. Thus, I_D/I_G ratio reflects the relative number of sp^3-carbon atoms on SWNTs, and it can be used further to indicate the functionalization. The RBM band intensity reduction could be also used as evidence of successful covalent functionalization.[51] Furthermore, the frequency of the tangential vibrational modes of the carbon atoms in the SWCNT-CHO shifted to higher frequencies compared to pristine SWCNTs (1589 cm^{-1}). Those shifts provide evidence for charge transfer between the dopant and the SWCNT. Due to the electron-acceptor character of the formyl group, electrons from the π-state carbon transfer to the doping functional group and create hole carriers in the SWCNTs. A similar situation was observed for chemical CNT doping with iodine and bromine.[52,53]

Conclusions

Rieche reaction was found as the most effective route of CNT formylation. The main advantages of this protocol include: a broad scope of non-disturbing functional groups possibly present in the pre-functionalized CNTs, lack of oxidative disruption of the CNT skeleton, lack of necessity of operating with carcinogenic chromium(VI) compounds and, last but not least, the one-step, one-pot synthetic procedure based on a wet workup. Moreover, the relative reactivity of in-house and Nanocyl MWCNTs resembles our findings from 1,3-dipolar cycloaddition of nitrile *N*-oxides to nanotubes,[54] confirming that such thinner MWCNTs are *ca.* thrice more reactive, as shown here, against electrophiles.

Conflicts of interest

There are no conflicts to declare.

Acknowledgements

The authors are greatly indebted to Silesian University of Technology (BKM-530/RCH2/2016), National Science Centre and The National Centre for Research and Development (TANGO, TANGO1/266702/NCBR/2015), both Poland. Golden Open Access mode for this work was generously supported from Silesian University of Technology Rector Pro-Quality Grant No. 04/020/RGJ17/0038. Moreover authors acknowledge Dr Eng. Dawid Janas for Raman spectra.

References

1 Y.-P. Sun, K. Fu and W. Huang, *Acc. Chem. Res.*, 2002, **35**, 1096–1104.
2 S. Mallakpour and S. Soltanian, *RSC Adv.*, 2016, **6**, 109916–109935.
3 L. Meng, C. Fu and Q. Lu, *Prog. Nat. Sci.*, 2009, **19**, 801–810.
4 B. Smith, *et al.*, *Langmuir*, 2009, **25**, 9767–9776.
5 N. P. Blanchard, R. A. Hatton and S. R. P. Silva, *Chem. Phys. Lett.*, 2007, **434**, 92–95.
6 H. Hiura, T. W. Ebbesen and K. Tanigaki, *Adv. Mater.*, 1995, **7**, 275–276.
7 Y. Peng and H. Liu, *Ind. Eng. Chem. Res.*, 2006, **45**, 6483–6488.
8 J. M. Simmons, *et al.*, *J. Phys. Chem. B*, 2006, **110**, 113–118.
9 J. L. Bahr, *et al.*, *J. Am. Chem. Soc.*, 2001, **123**, 6536–6542.
10 J. L. Bahr and J. M. Tour, *Chem. Mater.*, 2001, **13**, 3823–3824.

11 C. A. Dyke and J. M. Tour, *J. Am. Chem. Soc.*, 2003, **125**, 1156–1157.
12 Y. Chen, *et al.*, *J. Mater. Res.*, 1198, **13**, 2423–2431.
13 M. Holzinger, *et al.*, *Angew. Chem., Int. Ed.*, 2001, **40**, 4002–4005.
14 K. A. Worsley, K. R. Moonoosawmy and P. Kruse, *Nano Lett.*, 2004, **4**, 1541–1546.
15 M. J. Moghaddam, *et al.*, *Nano Lett.*, 2004, **4**, 89–93.
16 G. Viswanathan, *et al.*, *J. Am. Chem. Soc.*, 2003, **125**, 9258–9259.
17 S. Pekker, J. P. Salvetat, E. Jakab, J. M. Bonard and L. Forro, *J. Phys. Chem. B*, 2001, **105**, 7938–7943.
18 N. Tagmatarchis, V. Georgakilas, M. Prato and H. Shinohara, *Chem. Commun.*, 2002, 2010–2011.
19 N. Karousis and N. Tagmatarchis, *Chem. Rev.*, 2010, **110**, 5366–5397.
20 P. C. Ma, J.-K. Kim and B. Z. Tang, *Carbon*, 2006, **44**, 3232–3238.
21 J.-P. Tessonnier, A. Villa, O. Majouler, S. S. Su and R. Schlogl, *Angew. Chem.*, 2009, **48**, 6543–6546.
22 W. F. Tuley and R. Adams, *J. Am. Chem. Soc.*, 1925, **47**, 3061–3068.
23 M. R. Johnson and B. Rickborn, *J. Org. Chem.*, 1970, **35**, 1041–1045.
24 J. K. Whitesell and M. A. Whitesell, *Synthesis*, 1983, **1983**, 517–536.
25 A. F. Abdel-Magid, K. G. Carson, B. D. Harris, C. A. Maryanoff and R. D. Shah, *J. Org. Chem.*, 1996, **61**, 3849–3862.
26 E. J. Corey, N. W. Gilman and B. E. Ganem, *J. Am. Chem. Soc.*, 1968, **90**, 5616–5617.
27 L. Saikia, J. M. Baruah and A. J. Thakuri, *Org. Med. Chem. Lett.*, 2011, **1**, 1–6.
28 E. Abele, R. Abele and E. Lukevics, *Chem. Heterocycl. Compd.*, 2004, **40**, 1–15.
29 B. E. Maryanoff and A. B. Reitz, *Chem. Rev.*, 1989, **89**, 863–927.
30 J. Dambacher, *et al.*, *Tetrahedron Lett.*, 2005, **46**, 4473–4477.
31 J. C. Gilbert and U. Weerasooriya, *J. Org. Chem.*, 1982, **47**, 1837–1845.
32 M. Davoust, J.-F. Briere, P.-A. Jaffres and P. Metzner, *J. Org. Chem.*, 2005, **70**, 4166–4169.
33 A. Piccinini, S. A. Kavanagh, P. B. Connon and S. J. Connon, *Org. Lett.*, 2010, **12**, 608–611.
34 M. K. Bayazit, A. Suri and K. S. Coleman, *Carbon*, 2010, **48**, 3412–3419.
35 A. Suri and K. S. Coleman, *J. Nanosci. Nanotechnol.*, 2012, **12**, 2929–2933.
36 L. Moradi, N. Izadi and F. Rostami, *Int. J. Biomed. Nanosci. Nanotechnol.*, 2015, **11**, 93–99.
37 L. Moradi and I. Etesami, *Fullerenes, Nanotubes, Carbon Nanostruct.*, 2016, **24**, 213–218.
38 P. C. Ma, J.-K. Kim and B. Z. Tang, *Carbon*, 2006, **44**, 3232–3238.
39 W.-X. Lou, *Synth. Commun.*, 1992, **22**, 767–772.
40 E. Santaniello and P. Ferraboschi, *Communications*, 1980, 646–647.
41 C. Li, *et al.*, *Synlett*, 2002, **12**, 2041–2042.
42 V. Rajeshkumar, Y. T. Lee and M. C. Stuparu, *Eur. J. Org. Chem.*, 2016, **2016**, 36–40.
43 Y. S. Kim, S. J. Yang, H. J. Lim, T. Kim and C. R. Park, *Carbon*, 2012, **50**, 3315–3323.
44 A. Misra, P. K. Tyagi, M. K. Singh and D. S. Misra, *Diamond Relat. Mater.*, 2006, **15**, 385–388.
45 V. T. Le, *et al.*, *Adv. Nat. Sci.: Nanosci. Nanotechnol.*, 2013, **4**, 035017.
46 S. Boncel, *et al.*, *ACS Biomater. Sci. Eng.*, 2016, **2**, 1273–1285.
47 F. Hennrich, *et al.*, *J. Phys. Chem. B*, 2005, **109**, 10567–10573.
48 M. S. Dresselhaus, G. Dresselhaus, A. Jorio, A. G. Souza Filho and R. Saito, *Carbon*, 2002, **40**, 2043–2061.
49 S. Costa, E. Borowiak-Palen, M. Kruszynska, A. Bachmatiuk and R. J. Kalenczuk, *Mater. Sci.-Pol.*, 2008, **26**, 433–441.
50 L. Bokobza and J. Zhang, *eXPRESS Polym. Lett.*, 2012, **6**, 601–608.
51 K. Zhang, Q. Zhang, C. Liu, N. Marzari and F. Stellacci, *Adv. Funct. Mater.*, 2012, **22**, 5216–5223.
52 A. M. Rao, P. C. Eklund, S. Bandow, A. Thess and E. E. Smalley, *Nature*, 1997, **388**, 257–259.
53 C. N. R. Rao and R. Voggu, *Mater. Today*, 2010, **13**, 34–40.
54 A. P. Herman and S. Boncel, *RSC Adv.*, 2016, **6**, 64129–64132.